CrystEngComm

COMMUNICATION

View Article Online
View Journal | View Issue

Cite this: *CrystEngComm*, 2018, **20**, 407

Received 6th November 2017,
Accepted 4th January 2018

DOI: 10.1039/c7ce01922j

rsc.li/crystengcomm

Efficient removal of low concentration methyl mercaptan by HKUST-1 membrane constructed on porous alumina granules†

Xiang Ma, [abc] Shengpan Peng,[abc] Weiman Li,[abc] Haidi Liu[ac] and Yunfa Chen*[ac]

A HKUST-1 metal–organic framework membrane was constructed on porous Al_2O_3 granules for the first time for the removal of low concentration CH_3SH. The granules exhibited higher sulfur capacity than the pure HKUST-1 powders owing to the excellent dispersion of the MOF membrane on the Al_2O_3 substrate. The granules also showed good water resistibility.

Methyl mercaptan (CH_3SH) is a kind of typical volatile organosulfur odor in natural gas, petroleum gas, and water gas with a smell like that of rotten or cooked cabbage. In particular, industrial units such as pharmaceutical factories, insecticide factories and dyestuff plant using thiophene or thiocarbamide are troubled with serious odor problems. Municipal wastewater treatment plants also emit odors and appropriate deodorization methods are used.[1] Gas purification techniques such as adsorption, photocatalytic oxidation, biological degradation, thermal decomposition, and catalytic oxidation are emphasized to resolve the challenges aroused by this air pollutant.[2–6] However, there are a variety of advantages and disadvantages manifested by these techniques, and they show different degrees of cost effectiveness. For example, biological degradation requires a bioreactor with an associated aeration system, which is expensive. Photocatalytic oxidation needs high maintenance and high system control to avoid residual ozone. Catalytic oxidation has high ongoing chemical costs with the storage and handling of hazardous chemicals. Furthermore, all the methods mentioned above except for the adsorption technique could successfully reduce the CH_3SH concentration in gas flow from 100 ppm to 10 ppm; these methods, however, could hardly remediate gas with low CH_3SH concentrations (<10 ppm) to odorless. In terms of the adsorption technique, the adsorption capacity of materials and the removal of CH_3SH at low concentrations remain a challenge because the CH_3SH molecule is small in size so is not strongly retained on the surface of the adsorbents. This requires adsorption media with highly polar/hydrophilic surface features, which can induce reactive adsorption through hydrogen bonding, complexion and acid–base reactions.[7–9]

Metal–organic frameworks (MOFs) are emerging as a class of very important materials offering high levels of porosity with considerable control over pore size and composition.[10–12] Their potential versatility, especially in adsorption of airborne pollutants due to high selectivity, chemical and thermal stability in the low and mid temperature range, moderate heat of adsorption, and enhanced mass uptake, give them advantages over other porous materials such as activated carbon and zeolite.[13,14] Adsorptive removal of sulfur-containing compounds by MOFs has received attention because of the increasingly stringent regulations for environmental protection.[15–17] HKUST-1 was one of the first investigated materials to be identified as having a remarkably high capacity for various organosulfur compounds. Petit *et al.* found that reactive adsorption occurred, resulting in the formation of CuS, when HKUST-1 was used to adsorb H_2S.[18] Li *et al.* carried out adsorption of H_2S, CH_3CH_2SH and CH_3SCH_3 present in natural gas by HKUST-1 and different adsorptive behavior of these sulfur compounds was found through breakthrough experiments.[19] In a recent study, we reported that a copper-based MOF HKUST-1 with controllable size and shape can successfully adsorb low concentrations of CH_3SH owing to the strong interaction between the unsaturated copper sites of HKUST-1 and the –SH group of CH_3SH.[20] However, in practical applications, the granulation process will lead to unnecessary loss of HKUST-1 powder. Moreover, the inside part of the HKUST-1

[a] *State Key Laboratory of Multiphase Complex System, Institute of Process Engineering, Chinese Academy of Sciences, Beijing, 100190, China. E-mail: yfchen@ipe.ac.cn*
[b] *University of Chinese Academy of Sciences, No. 19A Yuquan Road, Beijing, 100049, China*
[c] *Center for Excellence in Regional Atmospheric Environment, Institute of Urban Environment, Chinese Academy of Sciences, Xiamen, 361021, China*

† Electronic supplementary information (ESI) available. See DOI: 10.1039/c7ce01922j

adsorbents will be wasted owing to the collapse of the pore structure in the outside part during the CH_3SH adsorption process, resulting in poor usage efficiency of the HKUST-1 adsorbents. Moreover, the water resistibility remains a challenge because of the competitive adsorption of water molecules at the open metal copper sites.[21] Alumina oxide is widely used in practical applications because of its high mechanical strength, chemical stability and porous structure.[22–24] Herein, we prepared continuous HKUST-1 membranes on commercial porous alumina supports (denoted as HKUST-1@Al_2O_3) using secondary growth, which showed good mechanical stability and technical feasibility of the ceramic supports for scale-up. The HKUST-1@Al_2O_3 adsorbents exhibited higher sulfur capacity than that of the pure HKUST-1 powders owing to the excellent dispersion of the MOF membrane on the Al_2O_3 substrate. Furthermore, the granules showed good water resistibility, which is ascribed to the hydroscopicity of porous alumina.

To fabricate the HKUST-1 membrane, a thermal seeding-mediated secondary growth strategy was employed, as illustrated in Fig. 1.[25] Firstly, the as-synthesized crystals of HKUST-1 along with excessive organic ligands and Cu species in the seed suspension were poured on the hot Al_2O_3 supports. Then, the seed-deposited Al_2O_3 was treated by secondary growth of HKUST-1 under hydrothermal conditions to form a continuous membrane. The whole seeding and growing process were accompanied with an obvious color change whereby the Al_2O_3 granules varied from white to green during the seeding process, and then to blue during the growing process, confirming the success of the thermal seeding and growth of HKUST-1 membrane procedure (see the synthetic details in the ESI†).

The morphologies and microstructures of the alumina support and HKUST-1@Al_2O_3 were examined by SEM. The as-synthesized crystals of HKUST-1 show octahedron crystalline morphology with size of about 2 μm by hydrothermal method (as shown in Fig. S1†). The SEM images of bare Al_2O_3 and seed-mediated Al_2O_3 are shown in Fig. 2a and b, respectively. The comparison between bare Al_2O_3 and seed-mediated Al_2O_3 exhibited the presence of seed crystals of HKUST-1 uniformly attached to the Al_2O_3 surface, which made the surface of Al_2O_3 less rugged. The top-view SEM image revealed that

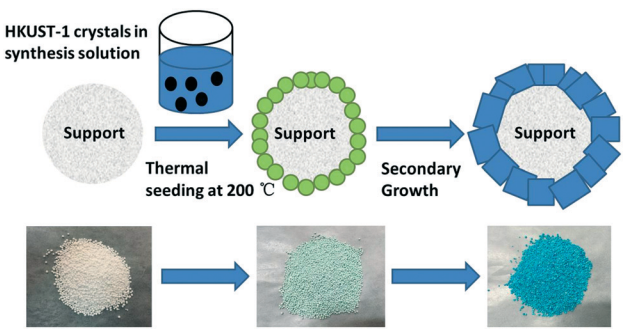

Fig. 1 Schematic illustration of the synthesis procedure of HKUST-1 membranes on alumina granules.

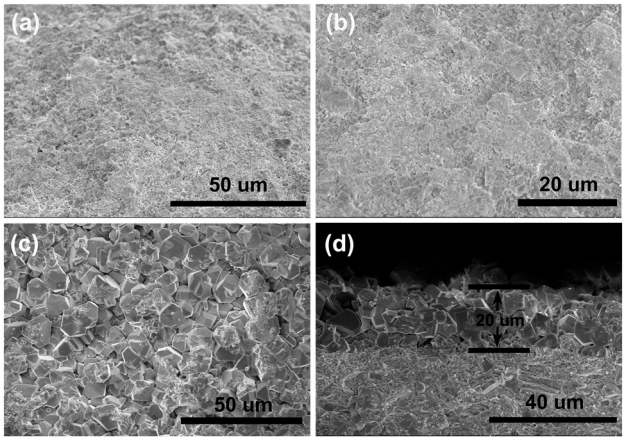

Fig. 2 SEM images of (a) Al_2O_3 support, (b) seed layers on Al_2O_3, (c) top views of HKUST-1@Al_2O_3, and (d) cross-section of HKUST-1@Al_2O_3.

HKUST-1@Al_2O_3 consisted of well-grown crystals fully covering the Al_2O_3 substrate surface, which is shown in Fig. 2c.

This membrane is continuous, without any cracks or pinholes. The cross-section image shown in Fig. 2d also illustrates the well-grown crystals on the substrate. The crystals were randomly oriented along the surface of the Al_2O_3. The thickness is about 20 μm for the MOF layer. The good dispersion of the HKUST-1 layer is favorable for the gas adsorption process.

The crystallographic structures of the alumina support and HKUST-1@Al_2O_3 materials were determined by XRD measurements. Fig. 3a illustrates the XRD patterns of the alumina support, which is indexed to the orthorhombic phases of alumina oxide hydrate. The detected diffraction peaks of HKUST-1@Al_2O_3 in Fig. 3b are in good agreement with

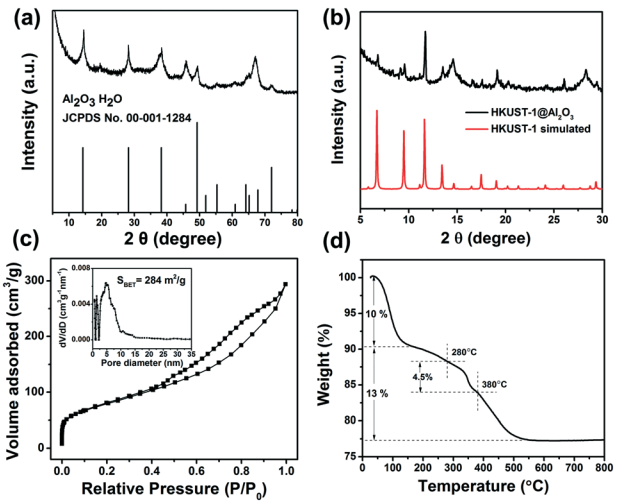

Fig. 3 XRD patterns of (a) Al_2O_3 support and (b) HKUST-1@Al_2O_3; (c) N_2 adsorption–desorption isotherm of HKUST-1@ Al_2O_3 (the inset is the corresponding DFT pore size distribution); (d) TGA curve of HKUST-1@Al_2O_3.

previously reported simulated HKUST-1 patterns, indicating the formation of a pure phase of HKUST-1 membrane.[26] It should be pointed out that the diffraction peaks of HKUST-1 were relatively weak because of the large content of alumina support. The porosity is considered as of paramount importance to the adsorption of hazardous pollutants. Fig. 3 displays the N_2 adsorption–desorption isotherms and the pore size distribution of the as-prepared HKUST-1@Al_2O_3. The pore diameter distributions of HKUST-1@Al_2O_3 consisted of two parts. One part is about 1 nm, which is in accordance with the structure of HKUST-1. The other part is located between 2 nm to 15 nm and is originated from the pores of the porous alumina support. The pores below 1 nm are absent for the bare alumina support (as shown in Fig. S2†). Moreover, the BET surface area of HKUST-1@Al_2O_3 is about 284 $m^2\ g^{-1}$ which is higher than that of the bare alumina support and an additional contribution to the adsorbed amount at very low relative pressure related to HKUST-1 was observed confirming the successful growth of the HKUST-1 membrane on the alumina substrate. The corresponding porosity data of HKUST-1@Al_2O_3 are summarized in Table S1.† The high surface area in synthesized HKUST-1@Al_2O_3 materials could provide more active sites and the highly porous structure would be more favorable for the adsorption and diffusion of reactant molecules. The loading amount of HKUST-1 is also considered as a paramount factor that affects the adsorption behavior of HKUST-1@Al_2O_3. Therefore, thermogravimetric analysis (TGA) was done for HKUST-1@Al_2O_3, bare alumina support and HKUST-1 and the results are shown in Fig. 3d and Fig. S3.† The loading amount of HKUST-1 on the alumina substrate is calculated through comparing the three TGA curves (as shown in ESI†). A four-step thermal decomposition process was observed for HKUST-1@Al_2O_3 that included the first weight loss of 10% from 40 to 150 °C, which is attributed to the loss of adsorbed H_2O and solvent molecules from both the alumina support and the HKUST-1 membrane. The second weight loss of about 2% between 150 °C to 280 °C resulted from the loss of adsorbed water and solvent molecules from the pores in the HKUST-1 membrane. The third weight loss of 4.5% between 280 °C to 380 °C is attributed to the decomposition of organic ligands of HKUST-1 (as shown in Fig. S3†). According to our calculation, the relative weight loss of the HKUST-1 crystals at this stage is approximately 60%, which is similar to the previously reported work,[27] roughly corresponding to the theoretical weight loss caused by the burning of the organic ligands in HKUST-1 in air (around 64% for the reaction $Cu_3(BTC)_2 \rightarrow Cu_2O$ and 60% for the reaction $Cu_3(BTC)_2 \rightarrow CuO$). Therefore, the loading amount of HKUST-1 membrane is about 7.5 wt% in the HKUST-1@Al_2O_3 adsorbents. The fourth weight loss of about 6.5% between 380 °C and 550 °C originated from the chemically bonded H_2O in the alumina support.[28]

CH_3SH breakthrough curves measured for the HKUST-1@Al_2O_3 and HKUST-1 under both dry and moist conditions are presented in Fig. 4a. The calculated breakthrough capacities of CH_3SH under dry and humid conditions are shown

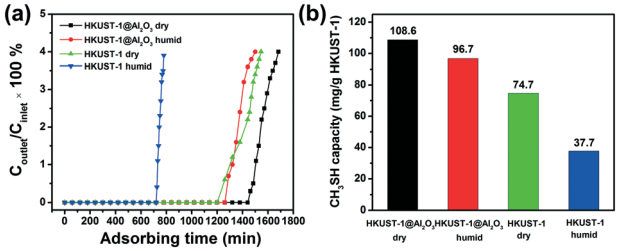

Fig. 4 (a) CH_3SH breakthrough curves and (b) CH_3SH adsorption capacity for the HKUST-1@Al_2O_3 and HKUST-1 composites measured under moist and dry conditions.

in Fig. 4b. The calculation of CH_3SH capacity is presented in the ESI.† The results indicate that the HKUST-1@Al_2O_3 composite is a better adsorbent than the bare HKUST-1 powders and exhibits good water resistibility. Under dry atmosphere conditions, the HKUST-1@Al_2O_3 material could last about 28 h till the outlet concentration reached the breakthrough value. It should be noted that the breakthrough time is longer than that of bare HKUST-1, although the content of HKUST-1 (about 75 mg) of HKUST-1@Al_2O_3 is lower than that of bare HKUST-1 (100 mg). The excellent dispersion of the HKUST-1 membrane on the Al_2O_3 substrate enhances the use efficiency of HKUST-1 because the mass transfer resistance for the 40–60 mesh HKUST-1 powders is higher than that of the uniform membrane, especially in low concentration CH_3SH gas flow conditions. Moreover, because the adsorption of CH_3SH could give rise to obvious damage to the HKUST-1 structure, the damaged outside part of HKUST-1 would hinder the transfer of CH_3SH towards the inside of the HKUST-1 powders. Under humid atmosphere conditions, the bare HKUST-1 powders performed worst in the adsorption process, which is ascribed to the competitive adsorption of H_2O molecules to the open metal copper sites, leading to a decrease in the number of active sites in the HKUST-1 materials. The CH_3SH capacity is 50% lower than that of bare HKUST-1 under dry conditions. Interestingly, the HKUST-1@Al_2O_3 composite under humid conditions performed only a little worse than that under dry conditions, probably because the hydroscopicity of porous alumina, which leads to competitive adsorption of water between HKUST-1 membrane and alumina (as shown in the TGA curve of bare alumina oxide below 150 °C), could reduce the adsorption of water on the HKUST-1 membrane. Therefore, the CH_3SH capacity is only 10% lower than that under dry conditions, indicating the good water resistibility of HKUST-1@Al_2O_3. Comparison of the sulfur compound capacity between HKUST-1@Al_2O_3 and previously reported work is summarized in Table S2.† The CH_3SH capacity of HKUST-1@Al_2O_3 is higher than that of most other sulfur compounds, such as SO_2, C_2H_5SH, CH_3SCH_3 and dibenzothiophene, adsorbed on HKUST-1. It is comparable to that of H_2S adsorbed on HKUST-1 combined with GO because the introduction of modified GO can lead to the formation of new micropores as a result of linkages between the sulfonic acids and amine groups of

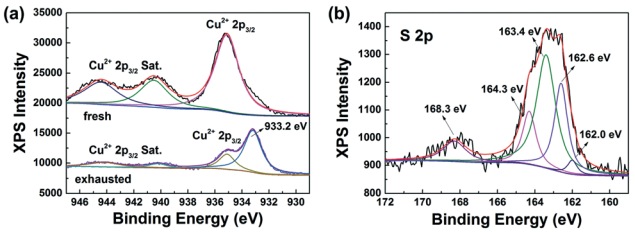

Fig. 5 (a) XPS spectra for Cu $2p_{3/2}$ of fresh and exhausted HKUST-1 and (b) XPS spectra for S 2p of exhausted HKUST-1.

modified GO and copper sites in HKUST-1. The breakthrough curve of the bare alumina support is presented in Fig. S4,† indicating that the alumina support is inactive for adsorbing CH_3SH. The top view SEM image of HKUST-1@Al_2O_3 after CH_3SH adsorption process is shown in Fig. S5.† The MOF membrane structure was well kept, indicating the good structural stability of the HKUST-1@Al_2O_3 composites. The HKUST-1@Al_2O_3 granules exhibiting high CH_3SH capacity with good water resistibility are applicable to a broad range of applications with varied operation conditions.

To determine the desulfurization mechanism, we characterized the exhausted samples through XPS measurements and compared the results against fresh samples using bare HKUST-1 materials (Fig. 5). Assignments of separate peaks in the XPS Cu $2p_{3/2}$ and S 2p spectra are listed in Table S3.† The Cu $2p_{3/2}$ spectrum of the fresh HKUST-1 is in accordance with that in the literature[29] while the Cu $2p_{3/2}$ spectrum of exhausted sample was quite different from the fresh one with the appearance of CuS located at 933.2 eV.[30] The S 2p spectrum of the exhausted sample was fitted into two pairs of $2p_{3/2}$ and $2p_{1/2}$ doublets. The first pair located at 162 eV and 162.6 eV is attributed to surface tangling sulfur anions, and the second pair located at 163.4 eV and 164.3 eV is assigned to the lattice sulfur of CuS in the surface region.[31,32] The peak located at 168.3 eV is assigned to the adsorbed methyl thiolate.[33] Apparently, CuS was formed during adsorption, coinciding with the colour change of HKUST-1 before and after the adsorption process.

The synthesized HKUST-1 materials have open sites of copper that exhibit Lewis acidity and, thus, the ability to adsorb compounds with lone electron pairs, such as sulfur compounds. The small size of CH_3SH molecules and the small hydrogen atom bound to sulfur at the end make it easy to access the open copper sites by coordination. Upon extended exposure to CH_3SH, the strong affinity between copper and sulfur may break the original Cu–O bond, form a new bond (O–Cu–S–CH_3) and release carboxylic groups. A fraction of –SCH_3 can further break down, resulting in the formation of CuS. Nevertheless, because the binding energy of S in O–Cu–S–CH_3 might be very close to that of CuS,[34] XPS results could not show the difference between them. The reactive adsorption of CH_3SH molecules creates a different chemical environment for Cu and eventually results in the colour change of the HKUST-1 material.

Conclusions

In summary, a HKUST-1 MOF membrane is prepared by the thermal seed-mediated secondary growth strategy. Structural studies show that MOF crystals fully cover the surface of the substrate and form a continuous MOF membrane. In a low concentration CH_3SH adsorption experiment, the MOF membrane showed higher CH_3SH capacity and better water resistibility than the bare HKUST-1 powders. The sulfur compound capacity is higher than that of other previously reported works. Reactive adsorption was found because of the strong interaction between the unsaturated copper sites in HKUST-1 and the –SH group of CH_3SH, which resulted in the formation of CuS. The exceptionally high sulfur capacity and good water resistibility using alumina oxide as the substrate make this MOF membrane a very promising candidate for practical applications.

Conflicts of interest

There are no conflicts to declare.

Acknowledgements

We are grateful to the Strategic Project of Science and Technology of the Chinese Academy of Science (No. XDB05050400) and the National Science and Technology support (No. 2014BAC21B00).

Notes and references

1 P. Lewkowska, B. Ciešlik, T. Dymerski and P. Konieczka, *Environ. Res.*, 2016, **151**, 573–585.
2 T. X. Liu, X. Z. Li and F. B. Li, *Environ. Sci. Technol.*, 2008, **42**, 4540–4545.
3 X. Z. Li, M. F. Hou, F. B. Li and H. Chua, *Ind. Eng. Chem. Res.*, 2006, **45**, 487–494.
4 S. Z. Zhao, H. H. Yi, X. L. Tang, F. Y. Gao and B. W. Zhang, *J. Cleaner Prod.*, 2015, **87**, 856–861.
5 R. Lebrero, A. C. Gondim, R. Pérez, P. A. García-Encina and R. Muñoz, *Water Res.*, 2014, **49**, 339–350.
6 C. H. Tsai, W. J. Lee, C. Y. Chen and W. T. Liao, *Ind. Eng. Chem. Res.*, 2001, **40**, 2384–2395.
7 H. Tamai, H. Nagoya and T. Shiono, *J. Colloid Interface Sci.*, 2006, **300**, 814–817.
8 S. W. Lee, W. M. A. W. Daud and M. G. Lee, *J. Ind. Eng. Chem.*, 2010, **16**, 973–977.
9 S. Bashkova, A. Bagreev and T. J. Bandosz, *Catal. Today*, 2005, **99**, 323–328.
10 E. Barea, C. Montoro and J. A. R. Navarro, *Chem. Soc. Rev.*, 2014, **43**, 5419–5430.
11 P. Silva, S. M. F. Vilela, J. P. C. Tomé and F. A. A. Paz, *Chem. Soc. Rev.*, 2015, **44**, 6774–6803.
12 B. Li, H. M. Wen, Y. J. Cui, W. Zhou, G. D. Qian and B. L. Chen, *Adv. Mater.*, 2016, **28**, 8819–8860.
13 P. Sliva, S. M. F. Vilela, J. P. C. Tomé and F. A. A. Paz, *Chem. Soc. Rev.*, 2015, **44**, 6774–6803.

14 P. Kumar, K. H. Kim, E. E. Kwon and J. E. Szulejko, *J. Mater. Chem. A*, 2016, **4**, 345–361.
15 D. Britt, D. Tranchemontagne and O. M. Yaghi, *Proc. Natl. Acad. Sci. U. S. A.*, 2008, **105**, 11623–11627.
16 P. Z. Li, X. J. Wang, S. Y. Tan, C. Y. Ang, H. Z. Chen, J. Liu, R. Q. Zou and Y. L. Zhao, *Angew. Chem., Int. Ed.*, 2015, **54**, 1–6.
17 I. Ahmed, N. A. Khan and S. H. Jhung, *Inorg. Chem.*, 2013, **52**, 14155–14161.
18 C. Petit, B. Levasseur, B. Mendoza and T. J. Bandosz, *Microporous Mesoporous Mater.*, 2012, **154**, 107–112.
19 Y. Li, L. J. Wang, H. L. Fan, J. Shangguan, H. Wang and J. Mi, *Energy Fuels*, 2015, **29**, 298–304.
20 X. Ma, H. D. Liu, W. M. Li, S. P. Peng and Y. F. Chen, *RSC Adv.*, 2016, **6**, 96997–97003.
21 J. Liu, Y. Wang, A. I. Benin, P. Jakubczak, R. R. Wills and M. D. LeVan, *Langmuir*, 2010, **26**, 14301–14307.
22 M. C. Álvarez-Galván, B. Pawelec, V. A. de la Peña O'Shea, J. L. G. Fierro and P. L. Arias, *Appl. Catal., B*, 2004, **51**, 83–91.
23 J. P. Nan, X. L. Dong, W. J. Wang, W. Q. Jin and N. P. Xu, *Langmuir*, 2011, **27**, 4309–4312.
24 W. Lee and S. J. Park, *Chem. Rev.*, 2014, **114**, 7487–7556.
25 V. V. Guerrero, Y. Yoo, M. C. McCarthy and H. K. Jeong, *J. Mater. Chem.*, 2010, **20**, 3938–3943.
26 S. S.-Y. Chui, S. M.-F. Lo, J. P. H. Charmant, A. G. Orpen and L. D. Williams, *Science*, 1999, **283**, 1148–1150.
27 Y. T. Wang, Y. Y. Lu, W. W. Zhan, Z. X. Xie, Q. Kuang and L. S. Zheng, *J. Mater. Chem. A*, 2015, **3**, 12796–12803.
28 T. Morinoto, M. Nagao and J. Imai, *Bull. Chem. Soc. Jpn.*, 1971, **44**, 1282–128844.
29 A. S. Duke, E. A. Dolgopolova, R. P. Galhenage, S. C. Ammal, A. Heyden, M. D. Smith, D. A. Chen and N. B. Shustova, *J. Phys. Chem. C*, 2015, **119**, 27457–27466.
30 C. Y. Wu, S. H. Yu, S. F. Chen, G. N. Liu and B. H. Liu, *J. Mater. Chem.*, 2006, **16**, 3326–3331.
31 R. Cai, J. Chen, J. X. Zhu, C. Xu, W. Y. Zhang, C. M. Zhang, W. H. Shi, H. T. Tan, D. Yang, H. H. Hng, T. Mariana and Q. Y. Yan, *J. Phys. Chem. C*, 2012, **116**, 12468–12474.
32 S. L. Xiong and H. C. Zeng, *Angew. Chem., Int. Ed.*, 2012, **51**, 949–952.
33 S. Z. Zhao, H. H. Yi, X. H. Tang, F. Y. Gao, B. W. Zhang, Z. X. Wang and Y. R. Zuo, *J. Cleaner Prod.*, 2015, **87**, 856–861.
34 V. Srinivasan, E. I. Stiefei, A. Elsberry and R. A. Walton, *J. Am. Chem. Soc.*, 1979, **101**, 2611–2614.